# The critical slip distance for seismic and aseismic fault zones of finite width

**Chris Marone[1], Massimo Cocco, Eliza Richardson[1], and Elisa Tinti**

Istituto Nazionale di Geofisica e Vulcanologia, Rome, Italy
[1]Permanent address: Dept. of Geosciences, Penn State, USA

Submitted to Special Issue of PAGEOPH on
Fault-zone Properties and Earthquake Rupture Dynamics

Submitted 20 Feb. 2008, Revised 26 June 2008

**Abstract:**

We present a conceptual model for the effective critical friction distance for fault zones of finite width. A numerical model with 1D elasticity is used to investigate implications of the model for shear traction evolution during dynamic and quasi-static slip. The model includes elastofrictional interaction of multiple, parallel slip surfaces, which obey rate and state friction laws with either Ruina (slip) or Dieterich (time) state evolution. A range of slip acceleration histories are investigated by imposing perturbations in slip velocity at the fault zone boundary and using radiation damping to solve the equations of motion. The model extends concepts developed for friction of bare surfaces, including the critical friction distance $L$, to fault zones of finite width containing wear and gouge materials. We distinguish between parameters that apply to a single frictional surface, including $L$ and the dynamic slip weakening distance $d_o$, and those that represent slip for the entire fault zone, which include the effective critical friction distance, $D_{cb}$, and the effective dynamic slip weakening distance $D_o$. A scaling law for $D_{cb}$ is proposed in terms of $L$ and the fault zone width. Earthquake source parameters depend on net slip across a fault zone and thus scale with $D_{cb}$, $D_o$, and the slip at yield strength $D_a$. We find that $D_a$ decreases with increasing velocity jump size for friction evolution via the Ruina law, whereas it is independent of slip acceleration rate for the Dieterich law. For both laws, $D_a$ scales with fault zone width and shear traction exhibits prolonged hardening prior to reaching a yield strength. The parameters $D_{cb}$ and $D_o$ increase roughly linearly with fault zone thickness. This paper and a companion paper in the volume discuss the problem of reconciling laboratory measurements of the critical friction distance with theoretical- and field-based estimates of the effective dynamic slip weakening distance.

## 1. Introduction

The nature of the transition from interseismic fault creep to transiently-accelerating slip and dynamic rupture propagation is a central problem in earthquake science. Laboratory experiments, studies of frictional instability, and theoretical models confirm that strength breakdown and transient frictional behavior are fundamental to phenomena ranging from aseismic slip, earthquake nucleation, dynamic earthquake triggering, and postseismic fault slip (e.g., IDA, 1972; SCHOLZ, ET AL., 1972; DIETERICH, 1972, 1979; PALMER AND RICE, 1973; ANDREWS 1976A,B; RUINA, 1983; RICE AND RUINA, 1983; TULLIS AND WEEKS, 1986; TULLIS, 1988; MARONE ET AL., 1991; DIETERICH, 1992; TULLIS, 1996; BOATWRIGHT AND COCCO, 1996; BEELER ET AL., 1996; SLEEP, 1997; MARONE, 1998; SCHOLZ, 1998; RICHARDSON AND MARONE, 1999; BIZZARRI ET AL., 2001; COCCO AND BIZZARRI, 2002; LAPUSTA AND RICE, 2003; BIZZARRI AND COCCO, 2003; BOETTCHER AND MARONE, 2004; TINTI ET AL., 2005A,B; BHAT ET AL., 2007; SAVAGE AND MARONE, 2007; LIU AND RICE, 2007; AMPUERO AND RUBIN, 2008). In the context of rate and state friction laws, a key parameter determining transient slip behavior is the critical friction distance $L$ for breakdown of frictional strength. Rapid fault slip acceleration and earthquakes are favored by large ratios of dynamic stress drop to $L$, whereas transient slip, slow earthquakes and aseismic phenomena are favored by near zero and negative values of this ratio. The physical mechanisms governing the critical slip distance are poorly understood and the few available observations come from laboratory experiments on rock fracture and friction. Strength breakdown during preseismic and aseismic slip likely involves multiple processes, each with its own characteristic length and time scale. This implies that rupture nucleation and dynamic propagation are inherently scale dependent processes. In the present study, we focus on the length scale parameters and, in particular, on the slip associated with the breakdown phase.

In this paper, we distinguish between parameters that apply to a single frictional surface, including $L$ and the dynamic slip weakening distance $d_o$, and those that represent slip for the entire fault zone, which include the effective fault zone critical friction distance $D_{cb}$ and the effective dynamic slip weakening distance $D_o$. Earthquake source parameters depend on net slip across a fault zone and thus scale with $D_{cb}$, $D_o$, and the slip at yield strength $D_a$. We propose a scaling relation between $D_{cb}$ and the intrinsic critical friction distance for frictional contact junctions $L$. We posit that $D_{cb}$ is a key parameter determining rupture acceleration, dynamic rupture propagation, and the mechanical energy absorbed within the fault zone. In a companion paper, COCCO ET AL. (2008, this volume) investigate the dynamic slip weakening parameter $D_c$, which we refer to as $D_o$ in this paper.

The pioneering laboratory friction experiments of RABINOWICZ (1951) showed that the transition between static and dynamic friction occurs over a characteristic slip ($s_k$ see Figure 1a). This concept has been incorporated in frictional instability models (PALMER AND RICE, 1973) and theoretical slip-weakening laws (IDA, 1972; ANDREWS 1976a,b). However, only the rate- and state-dependent friction laws (DIETERICH 1979; RUINA, 1983; RICE AND RUINA, 1983), distinguish between the characteristic length scale of the constitutive formulation ($L$, see Figure 1c) and the slip weakening distance of shear traction evolution ($d_o$, see Figure 1c). By modeling the dynamic propagation of a shear crack governed by rate- and state-dependent friction COCCO AND BIZZARRI (2002) and BIZZARRI AND COCCO (2003) proposed a scaling law for $L$ and $d_o$.

The overall behavior of shear stress breakdown and friction evolution is commonly named dynamic fault weakening (e.g., RICE AND COCCO, 2006; COCCO AND TINTI, 2008). The physical interpretation of the length scale parameters characterizing dynamic fault weakening depends on the adopted fault mechanical model and the processes controlling friction evolution. In the framework of a fault zone model consisting of two surfaces in contact, the

parameter $L$ is commonly interpreted as the slip necessary to renew the population of contacts and $d_o$ is a parameter contributing to the energy necessary to maintain dynamic crack propagation (i.e., fracture energy). However, in a more complex fault zone model of finite thickness and heterogeneous strain localization, as indicated by geological observations of faults (e.g., CHESTER ET AL., 1993; COWAN, 1999; SIBSON, 2003, BILLI AND STORTI, 2004; CASHMAN ET AL., 2007), the physical interpretation of the constitutive parameter $L$ and of the critical slip weakening distance is not straightforward (e.g., ANDO AND YAMASHITA, 2007; BHAT ET AL., 2007).

At seismic rupture speeds, breakdown weakening processes may include failure of adhesive contact junctions, yielding of grain cements, flash heating, particle fracture, and shear-induced melting (e.g., DI TORO ET AL., 2006; RICE, 2006; NIELSEN ET AL., 2008; BEELER ET AL., 2008). At slower rates, such as appropriate for earthquake nucleation and aseismic creep, breakdown weakening may include mineral growth, shear localization, pressure solution creep, and reorganization of fault zone microstructures (e.g., *RUTTER ET AL., 1986; VAN DER PLUIJM ET AL., 2001; SOLUM ET AL., 2003; NIEMEIJER AND SPIERS, 2006; IKARI ET AL., 20*07). In laboratory experiments on bare rock surfaces sheared at slow rates (< 0.01 to 0.1 m/s) $L$ can be related to asperity contact junctions via concepts of Hertzian contacts (RABINOWICZ, 1951; SCHOLZ, 2002). When wear material is involved, processes involving granular physics become important, and higher strain rates mean that processes involving shear heating must be included (e.g., DI TORO ET AL., 2006).

We emphasize here that while the parameter $L$ is the intrinsic length scale for rate- and state-dependent friction, seismically-determined earthquake source parameters will depend on net slip across the fault zone and thus the effective fault zone critical friction distance $D_{cb}$ and the effective dynamic slip weakening distance $D_o$ (Figure 1d). $L$ is a constitutive parameter of laboratory inferred rate-and-state constitutive laws and describes

the transition from one frictional state (e.g., static contact or steady creep) to another; for example as measured during velocity step experiments (Figure 1c).

Comparison of field, laboratory, and numerical estimates of slip weakening distances reveals significant discrepancies (MARONE AND KILGORE, 1993; IDE AND TAKEO, 1997; GUATTERI ET AL., 2001; OHNAKA, 2003; MIKUMO ET AL., 2003). Although laboratory friction data are reasonably well described by the rate and state friction constitutive laws, many of the underlying processes are poorly understood. This complicates application of laboratory data to in-situ fault conditions, which span time scales from seismic to interseismic and include complex thermal, chemical, and hydraulic processes. For example, BIZZARRI AND COCCO (2006a, b) used rate- and state-dependent constitutive laws to investigate frictional heating and thermal pressurization during dynamic fault weakening. Their results clearly show that $D_o$ depends strongly on the hydraulic and thermal parameters of the fault zone. Moreover, analysis of the effective critical slip distance determined from seismological data reveals fundamental problems associated with resolution and scaling (GUATTERI ET AL., 2001; COCCO ET AL., 2008 this issue).

The purpose of this paper is to describe a frictional model for fault zones of finite width and summarize recent progress on understanding the critical slip distance. We focus in particular on the problem of reconciling laboratory measurements of the critical slip distance with theoretical- and field-based estimates. In addition, we compare and discuss laboratory friction measurements for slow slip rates (< 0.01 to 0.1 m/s) with those derived from experiments at high slip rates (> 1 m/s), which yield significantly larger values of $L$ and $D_o$.

## 2. Friction laws and the transition from static to kinetic friction

RABINOWICZ (1951) introduced the slip weakening parameter, $s_k$, in his seminal paper on the transition from static to kinetic friction. He was motivated by the implausibility of

simple static-kinetic friction models, which assume that friction changes instantaneously with the onset of slip, and he showed that $s_k$ could be understood in terms of asperity contact properties. RABINOWICZ (1951, 1956) also rejected purely velocity dependent friction models on the basis of their inability to describe the transition from static to kinetic friction (Figure 1a) and available data showing that friction was not a single valued function of sliding velocity (BOWDEN AND TABOR, 1950; for a summary see DOWSON, 1979). The simplest model representing strength evolution that is consistent with both laboratory data and theoretical work on crack tip stresses and elasto-dynamic rupture propagation is one in which details of the transient weakening are simplified to a linear trend over slip distance $s_k$ (Figure 1a).

A consequence of slip weakening behavior is the existence of a breakdown zone, which represents the spatial scale over which slip weakening occurs. BARENBLATT (1959) and IDA (1972) introduced the breakdown zone for tensile and shear cracks, respectively, to avoid infinitely large stress concentrations on the fracture plane. One form of the breakdown zone model involving linear slip weakening, such as in Figure 1a, has been widely adopted in the literature (IDA, 1972; PALMER AND RICE, 1973; ANDREWS, 1976a, b).

Modern friction laws account for differences between static and kinetic friction in addition to: 1) variation in kinetic friction with slip velocity and 2) frictional aging (Figure 1b) in which the static friction varies with waiting time (e.g., DIETERICH, 1972; BEELER ET AL., 1994; KARNER AND MARONE, 2001). The rate and state friction laws (for reviews see, *TULLIS* 1996; *MARONE*, 1998) combine aging, velocity-dependent kinetic friction, and observations of instantaneous friction rate effects (Figure 1c). These laws reproduce a wide range of laboratory observations and are capable of describing the full spectrum of fault behaviors, ranging from aseismic slip events to slow earthquakes and dynamic rupture (e.g., SCHOLZ, 2002).

In the context of rate and state friction, slip weakening represents a memory effect that fades with time and slip following a perturbation in slip velocity, normal stress or physical properties of the fault zone that are described by a friction state variable (Figure 1c). Rate and state friction behavior is characterized by three or more empirical parameters, which may be loosely thought of as material properties. These parameters vary with rock mineralogy, physicochemical conditions, and stressing rate of the frictional surface or shear zone, reflecting changes in the atomic and larger-scale processes of strain accommodation.

A major challenge in earthquake science is that of determining the in-situ conditions and frictional properties appropriate for a given fault zone and seismic or aseismic phenomena. It is important to relate the friction parameters to seismological parameters of stress drop, slip weakening, and breakdown work (TINTI et al., 2005. Figure 1d shows these parameters in the context of dynamic rupture modeling inferred from seismologic data. A companion paper (COCCO ET AL., 2008 this issue) focuses on these parameters and the problem of measuring slip weakening using seismic data and interpreting its scaling with other earthquake source parameters.

## 3. Contact model for the critical slip distance of solid surfaces and shear zones

RABINOWICZ (1951; 1958) showed that the slip weakening distance $s_k$ could be understood in terms of asperity contact properties. He proposed a model in which $s_k$ is proportional to contact junction size (Figure 2a) and slip weakening results from progressive reduction of the real area of contact and/or replacement of older, stronger contact area with newly created, weaker contact (Figure 2b). This model is consistent with data showing that the rate-state friction parameter $L$ is proportional to roughness of clean solid surfaces and with measurements showing that $L$ scales with particle diameter of sheared granular layers (DIETERICH, 1981; MARONE AND KILGORE, 1993). The asperity model for $s_k$ and $L$ forms the

basis of a common interpretation of the state variable in rate and state friction laws as the average age of a contact given by the ratio of $L$ to slip velocity.

The contact junction model for $L$ (Figure 2a,b) can be extended to a granular shear zone (Figure 2c). We focus here on the case of a mature fault zone of finite width, where the width is many times larger than the average particle diameter. Shearing of the fault boundary is accomplished by slip increments within the zone, along surfaces between contact junctions. Figure 2c shows a simplified geometry in which contacts are subparallel to the shear zone boundaries (Figure 2d). The model is based on field and laboratory studies showing: 1) that shear becomes localized along boundary parallel planes that migrate throughout the zone with continued shear (e.g., MANDL ET AL., 1977; LOGAN ET AL., 1979; BEELER ET AL., 1996; MARONE, 1998), 2) the macroscopic coefficient of kinetic friction for a sheared granular layer is linearly related to particle contact dimensionality, such that friction of 1D grains is a factor of 3 lower than that for an assemblage of 3D spherical particles (FRYE AND MARONE, 2002; KNUTH AND MARONE, 2007); 3) the observation that the effective critical friction distance scales with shear zone thickness (MARONE AND KILGORE, 1992), and 4) Theoretical studies showing the necessity to identify finite length and time scale parameters for dynamic rupture (BHAT ET AL., 2007; ANDO AND YAMASHITA, 2007; COCCO AND TINTI, 2008). Frictional shear of the layer boundaries by a slip distance $x$ is the sum of slip increments $s$ on the number of contacts within the shear zone (Figure 2 c-e). This model links frictional behavior to dynamic rupture by defining a scaling of $L$ with breakdown work and related seismic parameters (COCCO ET AL., 2008 this issue).

For a fault zone of thickness $T$, the effective critical slip distance is given by the sum of contributions from individual contacts within the zone. We define the critical friction distance for a single contact as $L$. Then, $D_{cb} = n\, L\, \chi$, where $\chi$ is a geometric factor to account for contact orientation and $n$ is the number of surfaces in the shear zone (Figure 2). Particle

diameter $D$ can be related to $L$ via contact properties as: $L = D\ \zeta$, where $\zeta$ is a constant including elastic and geometric properties and the slip needed for fully-developed sliding at the contact (BOITNOTT ET AL., 1992). Combining these relations and the constants, we can define a linear relation between $D_{cb}$ and shear zone thickness as:

$$D_{cb} = T\ \gamma_c, \tag{1}$$

where $\gamma_c$ is the critical strain derived from slip increments on individual surfaces within the shear zone. This parameter is given by the product of $\chi$ and $\zeta$,and we expect that it varies with particle size, angularity, fault gouge mineralogy, and perhaps fault zone roughness. MARONE AND KILGORE (1993) determined $\gamma_c = 0.01$ using laboratory data on granular shear zones of varying thickness. Rewriting Equation (1) in terms of $L$ yields:

$$\gamma_c = n\ L\ \chi/T\ . \tag{2}$$

Thus, $\gamma_c$ is directly proportional to $L$.

Our proposed granular model for $D_{cb}$ retains the connection between slip velocity and contact lifetime suggested by RABINOWICZ (1951). If the boundary shearing velocity is $v$, the average interparticle slip velocity on surfaces within the shear zone is $v/n$ and the average contact lifetime is given by $L/v$. This result is consistent with studies showing that frictional memory effects –and the friction state variable– depend upon contact lifetime and also internal granular structure such as packing density, porosity, shear fabric, and granular force chains (e.g., MARONE ET AL., 1990; SEGALL AND RICE, 1995; BEELER ET AL., 1996; MAIR ET AL., 2002; MAIR AND HAZZARD, 2007).

## 4. Model for a shear zone of finite thickness

We investigate implications of a shear zone model in which slip occurs on multiple surfaces in a zone of finite thickness (Figure 2) and focus, in particular, on scaling of the critical slip distance with fault zone properties. Consider an idealized fault of width T within

a fractured host rock at Earth's surface (Figure 3). To account for both internal shear behavior and macroscopic properties of the fault zone, we assume the fault is composed of multiple, subparallel slip surfaces, each of which exhibits rate and state frictional characteristics (Figure 3b). We focus on mature faults that contain boundary parallel shear localization and we do not consider oblique shear bands such as Riedel shears. The fault zone is assumed to be symmetric about its midpoint $T/2$. Slip surfaces are separated by a distance $h$ and coupled elastically to adjacent surfaces via a stiffness $K_{int}$ (shown schematically as a leaf spring in Figure 3). The shear zone boundary is driven by remote loading at a constant tectonic displacement rate $v_{pl}$ and this elastic coupling is characterized by stiffness $K_{ext}$ (Figure 3). Our model is conceptually-similar to a Burridge-Knopoff model (BURRIDGE AND KNOPOFF, 1967) for a series of slider blocks linked by springs, except that the slider blocks in our model are in frictional contact and connected elastically in parallel rather than in series. Thus, slip on any surface within the fault zone reduces shear stress on all surfaces (Figure 3 inset). We assume stress equilibrium such that shear and normal stresses are equal on each surface. This simplified elastic model allows attention to focus on the role of friction parameters and fault zone width; future studies will incorporate models with internal stress/strength heterogeneity and variations in fault zone properties along strike.

For a given shear zone, slip is distributed along $n_s$ parallel surfaces and we index these surfaces with the parameter $i$, starting with $i = 0$ at the boundary. Each slip surface $i$ is coupled elastically to its neighbors via stiffness $K_{int}$. We take $K_{int} = G/h$, where $G$ is shear modulus and $h$ is layer spacing (Figure 3) and use $G = 30$ GPa and $h = 6$ mm. We explore a range of fault zone widths, but keep surface spacing $h$ constant. In the model results shown below, we assume that remote tectonic loading of the shear zone boundary is compliant relative to $K_{int}$ and fix the ratio $K_{int}/K_{ext}$ at 10. Another possibility, for future studies, would be to take $K_{int}/K_{ext}$ equal to the number of surfaces in the shear zone. Table 1 contains other

details of the parameters used.

Each surface $i$ in the shear zone exhibits rate and state frictional behavior, such that friction $\mu_i$ is a function of state $\theta_i$ and slip velocity $v_i$ according to:

$$\mu_i(\theta_i, v_i) = \mu_o + a\ ln\left(\frac{v_i}{v_o}\right) + b\ ln\left(\frac{v_o\theta_i}{L}\right) \tag{3}$$

where $\mu_o$ is a reference friction value at slip velocity $v_o$, and the parameters $a$, $b$, and $L$ are empirically-derived friction constitutive parameters, which we assume to be equal on all surfaces. Tectonic fault zones are likely to include spatial variations of the friction constitutive parameters within the shear zone, but these are beyond the scope of the present study. We analyze friction state evolution according to either:

$$\frac{d\theta_i}{dt} = 1 - \frac{v_i\theta_i}{L} \qquad \text{(Dieterich Law)} \tag{4}$$

or

$$\frac{d\theta_i}{dt} = -\frac{v_i\theta_i}{L} ln\left(\frac{v_i\theta_i}{L}\right). \qquad \text{(Ruina Law)} \tag{5}$$

Frictional slip on each surface satisfies the quasi-dynamic equation of motion with radiation damping:

$$\mu_i = \frac{\tau_o}{\sigma_n} - \frac{G}{2\beta\sigma_n}(v_i - v_{pl}) + k\ (v_{pl}\ t - v_i\ t) \tag{6}$$

where $\mu_i$ is the frictional stress, $\tau_o$ is an initial stress, $\beta$ is shear wave speed, $\sigma_n$ is normal stress, $k$ is stiffness divided by normal stress, and $t$ is time. We assume a normal stress of 100 MPa and define stiffness $k$ using this value (Table 1). Differentiating Equations 3 and 6 with respect to time and solving for $dv_i/dt$ yields:

$$\frac{dv_i}{dt} = \frac{k\,(v_{pl} - v_i) - \frac{b\frac{d\theta_i}{dt}}{\theta_i}}{\frac{a}{v_i} + \frac{G}{2\beta\sigma_n}}, \tag{7}$$

which applies for each surface within the shear zone. Our approach for including radiation damping (RICE, 1993) is similar to that described in previous works (PERFETTINI AND AVOUAC, 2004; ZIV, 2007).

We assume steady creep during the interseismic period and thus each surface of the fault zone undergoes steady state slip at velocity $v_i = v_o$ with $\mu_o = 0.6$ and $\theta_{ss} = L/v_o$. The effective stiffness $k_i$ between the load point and surface $i$ within the fault zone is given by:

$$\frac{1}{k_i} = \frac{1}{K_{ext}} + \sum_{j=1}^{i} \frac{1}{K_{int_j}} . \quad (8)$$

To determine shear motion within the fault zone, we solve the coupled equations (4) and (7) or (5) and (7) using stiffness from equation (8) and a 4th order Runga-Kutta numerical scheme. A perturbation in slip velocity is imposed at the shear zone boundary, via the remote loading stiffness $K_{ext}$ and for each time step in the calculation, the surface with the lowest frictional strength is allowed to slip. The initial conditions are that shear and normal stress are the same on each surface and thus we assume slip occurs where frictional strength is lowest. We ensure that time steps are small compared to the ratio of slip surface separation, $h$, to elastic wave speed. Thus, within a given time step, only one surface slips and it is coupled elastically to the remote loading velocity via the spring stiffness given in 8.

| *a* | *b* | *L (m)* | *h (m)* | $K_{ext}/\sigma_n$ $(m^{-1})$ | $n_s/2$ | *T (m)* | *v (m/s)* | *Model; Figure(s)* |
|---|---|---|---|---|---|---|---|---|
| 0.012 | 0.016 | 1e-5 | 6e-3 | 5e4 | 20 | 0.24 | 0.01 | 11.12_3; 4 |
| 0.012 | 0.016 | 1e-5 | 6e-3 | 5e4 | 10 | 0.12 | 0.01 | 11.12_4; 5 |
| 0.012 | 0.016 | 1e-5 | 6e-3 | 5e4 | 50 | 0.60 | 0.01 | 11.12_4; 6 |
| 0.012 | 0.016 | 1e-5 | 6e-3 | 5e4 | 60 | 0.72 | 0.01 | 13.12_4; 7 |
| 0.012 | 0.016 | 1e-5 | 6e-3 | 5e4 | 10-100 | Var. | Var. | 13.12; 8, 9, 10 |
| 0.012 | 0.016 | 1e-5-1e2 | 6e-3 | 5e4 | 20-40 | Var. | Var. | 3.2; 11 |
| 0.012 | 0.016 | 3e-5 | 6e-3 | 5e4 | 20 | 0.24 | 0.01 | 16.12; 12 |

**Table 1.** Model parameters. For all cases, G=30 GPa, σ = 100 MPa, $K_{int} = G/h$; $K_{int}/K_{ext}$ =10; $v_o$ = 1e-6 m. $n_s/2$ is the number of surfaces in the fault zone half width $T/2$.

## 5. Results

We adopt the constitutive parameters, elastic properties, and slip velocities used by COCCO AND BIZZARRI (2002). These parameters are consistent with laboratory friction data for bare rock surfaces and fault gouge for which shear is localized (MARONE ET AL., 1990; MAIR AND MARONE, 1999). COCCO AND BIZZARRI (2002) solved the elasto-dynamic equations for a 2D in-plane crack using a finite difference approach. They report traction evolution and slip histories for several cases. We use their peak dynamic slip velocities as a proxy for dynamic slip in our models. To initiate slip in the model, we apply a step change in loading velocity, as a proxy for arrival of dynamic rupture at a point on a fault undergoing steady slip. We compute the traction evolution as a function of slip at the shear zone boundary by summing the shear displacement on each internal surface. For reference, the traction evolution is also computed for a single surface with the same frictional properties (thin lines in Figure 4). Traction evolution as a function of slip for shear zones that are 24 cm wide and obey either the Ruina or Dieterich state evolution laws are shown in Figure 4; thick lines show traction at the center of the fault as a function of net slip at the boundary. Figure 4a shows the distinction between parameters that apply to a single frictional surface, including $L$ and the dynamic slip weakening distance $d_o$, and those that represent slip for the entire fault zone, which include the effective critical friction distance, $D_{cb}$, and the effective dynamic slip weakening distance $D_o$.

In our model, shear strength exhibits prolonged hardening prior to reaching a yield strength (thick lines in Figure 4). This arises in part because a perturbation in slip velocity, applied at the boundary, causes each surface in succession to accelerate and strengthen via the friction direct effect, given by the term $[a \ln(v/v_0)]$ in Equation (3). At each time step in the calculation, shear traction is equal on all surfaces as required by stress equilibrium, but only the weakest surface slips. Therefore, during the slip acceleration phase, any surface that

slips slightly more than surrounding surfaces has higher friction and the next slip increment occurs elsewhere. This ensures that shear is pervasive, and not localized, prior to peak yield strength. The peak yield strength is slightly lower for fault zones of finite width compared to the reference case due to greater state evolution in the shear zone compared to the reference fault with zero width.

We track the slip at peak friction, defined as $D_a$, and use it to characterize the slip hardening phase (COCCO ET AL., 2008). For shear zones that obey the Dieterich evolution law, the value of $D_a$ is much larger than that for the reference case (Figure 4a), although the post-peak strength evolution is not a function of shear zone thickness. The parameter $D_o$ corresponds to the slip during the dynamic stress drop (Figure 1d) for an elasto-dynamic model. We note that our parameter $D_o$ differs from studies of planar surfaces of zero thickness and some laboratory-based values (OHNAKA, 2003) for which the hardening phase and the parameter $D_a$ are near zero. In our notation, OHNAKA's (2003) parameter $D_c$ is given by: $D_c = D_o - D_a$. In our model, $D_o$ is given by the point at which friction reaches a minimum value after dynamic weakening. The hardening phase prior to reaching peak friction is shorter for the Ruina law than for the Dieterich law and the post-peak traction evolution also requires less slip (Figure 4b).

Figure 5 shows temporal evolution of friction and slip velocity for a shear zone that obeys the Ruina friction law and is 12 cm wide (10 surfaces in half width). The parameter $D_c$' is defined as the slip at peak velocity (MIKUMO ET AL., 2003; FUKUYAMA ET AL., 2005) and consistent with previous work (TINTI ET AL., 2004) is larger than $D_a$. The primary period of slip acceleration occurs during rapid weakening after the yield strength has been reached. Note that the friction and velocity curves of Figure 5 are normalized so that their maximum values are equal to 1.

Friction evolution varies systematically as a function of position within the shear zone

(Figure 6). The shear stress is equal on all surfaces of the fault zone at a given time; however frictional strength evolves according to slip velocity and state. Figure 6 shows details of the friction evolution for surfaces at distances of 6, 12, 18, 24, and 30 cm from the boundary (surface numbers 10, 20, 30, 40, and 50) for a shear zone of thickness 60 cm that contains 100 surfaces each of which follows the Ruina evolution law. The degree of hardening prior to reaching a yield strength increases with distance from the shear zone boundary and the yield strength decreases as the center of the shear zone is approached. These observations have important implications for seismological breakdown work, which is a more robust measure of fracture energy (COCCO AND TINTI, 2008), because traction evolution in the pre-yield stress region represents energy that derives from dynamic stress concentration at the rupture tip and is required to overcome local strength excess (COCCO ET AL., 2008). Note that slip velocity for the surface at the center of the shear zone, number 50 in Figure 6, exhibits slight overshoot and thus friction approaches the steady-state value from below.

For a point on a fault plane, slip velocity acceleration depends on several factors including rupture velocity, maximum particle velocity for the earthquake, and distance from the nucleation region. We consider a range of acceleration histories by applying velocity steps of different size to a model fault zone 72 cm thick with 120 surfaces. The far field load point velocity $v_{lp}$ is subject to step increases of ratio 10 to 10,000 relative to the initial value. The yield strength increases with velocity step size, as expected (Figure 7a). For Dieterich frictional state evolution, the parameter $D_a$ is constant, independent of acceleration history, whereas for Ruina state evolution $D_a$ decreases with increasing magnitude of the slip velocity perturbation (Figure 7b). These observations are consistent with results from solutions of the full elasto-dynamic equations for a 2D crack (BIZZARRI AND COCCO, 2003).

Details of the relationship between $D_a$, shear zone thickness, and slip velocity perturbation are shown in Figure 8. Symbols represent shear zones of different thickness; the

numbers at right represent the number of slip surfaces in the half width (Figure 8a). For the Ruina law, $D_a$ is nearly constant (ranging from 0 to 30 micron) with acceleration history for shear zones up to 36 cm wide (30 surfaces in the half width) and decreases with increasing velocity step size at a rate that scales directly with shear zone thickness (Figure 8b). Note that Figure 7 shows details of the traction evolution for one of the cases (T = 72 cm, 120 surfaces) shown in Figure 8. For the Dieterich law, $D_a$ is essentially independent of velocity step size for all shear zone thicknesses (Figure 8a).

Because seismological measurements of breakdown work include the contribution of traction evolution in the pre-yield stress region (COCCO ET AL., 2008), the differences between Dieterich and Ruina style frictional state evolution have important implications for scaling of dynamic rupture parameters with fault zone thickness. For Dieterich law state evolution on a fault zone that is 1.2 m wide, the ratio $D_a/D_o$ ranges from 0.57 to 0.75 for slip velocity jump ratios from 10 to 10,000, respectively, whereas for a 0.012 m wide fault zone, this ratio ranges from 0.05 to 0.10. For the same range of velocities and Ruina state evolution, a fault zone that is 1.2 m wide has $D_a/D_o$ ranging from 0.32 to 0.69, whereas a 0.012 m wide fault zone, has ratio from 0.04 to 0.10. This shows that pre-yield stress hardening increases with fault zone width and that the hardening phase can contribute up to 75% of the seismological breakdown work. Thus seismic energy radiation, which is proportional to dynamic stress drop, decreases with increasing breakdown work, because increasing breakdown work reduces the energy left to be radiated.

## 6. Implications for scaling of the dynamic slip weakening distance

COCCO AND BIZZARRI (2002) proposed a scaling relation between the critical friction distance $L$ and the dynamic slip weakening distance $d_o$. Written in terms of our variables, their scaling relation is: $d_o = L\ ln(v/v_o)$. Although the absolute values of $d_o$ obtained in our

model are approximate (because we do not solve the full elasto-dynamic equations of motion) the relative values are meaningful because our model includes radiation damping and uses model parameters obtained by COCCO AND BIZZARRI (2002), who solved the elasto-dynamic equations for a 2D in-plane crack.

For a fault zone of finite width, the critical friction distance and the dynamic slip weakening distance are given by $D_{cb}$ and $D_o$, respectively. These parameters are proportional to the net slip across the fault zone (Figure 4). Thus, we extend the scaling relation of COCCO AND BIZZARRI (2002) to obtain a relation between $D_o$ and $D_{cb}$:

$$D_o = D_{cb}\, ln(v/v_o). \tag{9}$$

This relation can be modified to include the effects of fault zone thickness, by noting that $D_{cb}$ scales with $T/h$: $D_o \approx L\ T/h$. Written in terms of the fault zone thickness and the intrinsic critical friction distance the scaling relation of COCCO AND BIZZARRI (2002) predicts a linear scaling relation between $D_o$ and fault zone thickness for a given intrinsic critical friction distance.

We may test the validity of this scaling relation in the context of our fault zone model by evaluating the scaling of $D_o$ with velocity step size and fault zone thickness (Figure 9). The plot symbols distinguish the number of shear zone surfaces (proportional to thickness) with the numbers at right in Figure 9a denoting surface number relative to the shear zone boundary (see Table 1 for model details). For the Dieterich law, $D_o$ increases with shear zone thickness and velocity step size (Figure 9a). This is consistent with the observation that $D_a$ is independent of velocity step size (Figure 7) because the rate of post yield stress weakening is independent of acceleration history in this case. For Ruina friction state evolution, $D_o$ exhibits more complex behavior. For thin shear zones (0-30 surfaces in half width $T/2$) $D_o$ is nearly independent of velocity step size; whereas for thicker zones (60+ surfaces in half width $T/2$), $D_o$ first decreases and then increases with increasing velocity step

size. For the parameters of our model, the minimum $D_o$ in the Ruina case occurs for a 300x velocity jump (Figure 9c). Thus, when frictional state evolves according to the Dieterich law the linear scaling between fault zone slip weakening distance and $D_{cb}$ predicted by Equation 9 is confirmed. In contrast, when state evolves with the Ruina law $D_o$ depends on $T$ as predicted but the relationship between $D_o$ and velocity perturbation is more complex than indicated in Equation 9. We find that both $D_o$ and $D_a$ vary with shear zone thickness and slip acceleration history (Figures 6 and 7). It is of interest to distinguish the proportion of the change in dynamic slip weakening distance associated with hardening, as measured by $D_a$ (Figure 9). For the Dieterich law, the difference $D_o$-$D_a$ increases with velocity jump size (Figure 9b) whereas for the Ruina law, this difference is relatively insensitive to velocity jump size and show more complex behavior (Figure 9d). These comparisons are useful for understanding the connection between our modeling results and laboratory measurements of the critical friction distance and slip weakening distance (e.g., MARONE AND KILGORE, 1993; OHNAKA, 2003).

We can further evaluate the scaling between fault zone thickness and the parameters $D_o$ and $D_a$. Figure 10 shows this relationship for velocity steps of 10x, 300x, and 10000x and fault zone thicknesses from 12 cm to 1.2 m (see Table 1 for other model parameters). For the Dieterich law, both $D_o$ and $D_a$ increase with thickness and $D_o$ increases with velocity jump size (Figure 10a and c). This is consistent with Equation 9 and expected from the traction evolution curves shown in Figure 7a. Friction evolution via the Ruina law shows that the dynamic slip parameters increase with fault zone thickness (Figure 10b,d) but smaller velocity jumps lead to greater $D_a$ (Figure 10b) and the dependence of $D_0$ on velocity step size is complicated and nonlinear (Figure 10d). Equation 9 also predicts scaling among $L$, $T$, and velocity jump ratio. Figure 11 shows this relationship for a range of $L$ values for two fault zone widths and two velocity jump ratios. (see Table 1 for other model parameters). For the

Ruina law, both $D_o$ and $D_a$ scale with $L$ and the magnitude of the velocity perturbation (Figure 11a and c). For the Dieterich law, $D_o$ and $D_a$ scale with $L$, but velocity perturbation magnitude has no effect (Figure 11b and d). For both state evolution laws, the effects of fault zone thickness and velocity perturbation are small compared to the effect of $L$.

## 7. Discussion

The ontogeny of large tectonic faults, coupled with wear and gouge formation during subsequent offset, means that earthquakes occur within fault zones of finite width. Although there is significant uncertainty about the width of active slip during dynamic rupture, many lines of evidence suggest that average fault zone width is 10's or 100's of cm or more. Our modeling results show that the critical slip distance, as measured at the fault zone boundary, scales with fault zone thickness. This result is robust for fault zones that obey rate and state friction because the only requirement is positive instantaneous friction rate dependence (positive $a$ in Equation 3). Indeed, positive values of this parameter are one of the most consistent observations from laboratory friction studies (e.g., MARONE, 1998; BEELER ET AL., 2008) and are confirmed by frictional stability analyses.

Due to the difficulty of measuring the shear zone critical friction distance, $D_{cb}$ directly, we focus on the closely related parameters $D_a$ and $D_o$ (Figure 1). Each of these slip distances is expected to scale with fault width $T$, independent of the friction state evolution law. We studied the role of slip acceleration by imposing step changes in slip velocity of varying magnitude at the shear zone boundary and found marked differences between the Dieterich and Ruina friction evolution laws (see Figures 7 and 8). Our results are consistent with those of an elasto-dynamic model (COCCO AND BIZZARRI, 2002; BIZZARRI AND COCCO; 2003) even though we use a simplified 1D elastic model. We show that $D_a$ decreases with increasing velocity jump size for friction evolution via the Ruina law (Figures 7b, 8b),

whereas it is independent of slip acceleration rate for the Dieterich law (Figures 7a and 8a). This is consistent with expectations from Equations (4) and (5) because frictional weakening requires a constant slip, independent of acceleration time, for the Dieterich law, whereas the rate of weakening scales strongly with slip velocity for the Ruina law (e.g. AMPUERO AND RUBIN, 2008). For our purposes, the scaling of $D_a$ with velocity perturbation size means that breakdown work and traction evolution during dynamic rupture will differ for the two friction laws. This further complicates the problem of relating seismic estimates of the slip weakening distance to physical models and laboratory measurements of $L$ (COCCO ET AL., 2008, this issue).

Another goal in evaluating the mechanics and scaling of slip weakening is that of relating laboratory data and seismic measurements of $D_{cb}$ to field observations of faulting. An understanding of shear zone width, particle size distribution, slip distribution, strain rate, and shear induced melting would be a major advance in understanding earthquakes. Our model provides a connection between friction constitutive parameters and fault strain profiles (Figure 12). In this example, the slip distribution across the shear zone is determined by summing slip increments on each of the surfaces within a zone containing 40 slip surfaces. This snapshot in time represents the slip distribution when boundary slip had just reached $D_a$ and thus shear traction was at the yield stress. In our model, subsequent slip after this point is concentrated on a single surface at the center of the fault zone.

The strain rate profile represents the average value of strain rate over the time interval from zero to the point at which stress reached the yield stress (Figure 12). Because of shear localization, the strain rate peak seen at the center of the shear zone (Figure 12) becomes larger with additional slip after the yield stress. Our model results for fault zone strain rate are generally consistent with field observations and indicate the importance of the transition from pervasive to localized shear within a fault zone. There is clearly a need to extend this

approach, to investigate the strain distribution after the full seismic slip. That would require some form of pre-determined localization dimension, for example by coupling slip on a subset of surfaces, or the inclusion of post yield stress slip hardening, so as to inhibit localized slip under some conditions. Shear heating or hydromechanical effects are obvious directions for future work.

Our simulations show a scaling of $D_o$ versus fault zone thickness $T$ (Figure 10). For $T$ ranging between 0.1 and 2 m $D_o$ ranges between 0.01 and 0.2 mm. The latter range is smaller than estimates based on seismological investigations (IDE AND TAKEO, 1997; GUATTERI ET AL., 2001; MIKUMO ET AL., 2003; SPUDICH AND GUATTERI, 2004; FUKUYAMA ET AL., 2005; FUKUYAMA AND MIKUMO, 2007; COCCO ET AL., 2008) and theoretical models (TINTI ET AL., 2004) as well as those inferred from high velocity friction experiments (HIROSE AND SHIMAMOTO, 2005; DI TORO ET AL., 2006), where $D_o$ is on the order of meters. There are two explanations for this discrepancy. The first relies on the effects of other processes that produce larger $D_o$ values from slip weakening curves. Thermal pressurization for instance (see BIZZARRI AND COCCO, 2006a,b) produces larger values of $D_o$ than those resulting from a simple rate and state friction model. Indeed, it is interesting to note that in order to have $D_o$ values or the order of meters, following our scaling law of Equation 9, the fault zone critical friction distance is required to be in the range of cm for expected values of the velocity jump ratio. This is larger than values commonly inferred from low speed velocity stepping friction experiments on gouge (MAIR AND MARONE, 1999). Other processes such as melting or silica-gel creation might also contribute to larger values of $L$ and $D_{cb}$. It is also possible that $D_{cb}$ is significantly larger in real dynamic fault weakening episodes, because slip velocity is far from a simplistic step function. The second explanation relates to the definition of fault zone thickness. In our study we define the fault zone thickness as the zone where contacts among gouge grains are distributed. Thus, this would correspond to the fault core thickness. In this

case, the proposed range of variability for T agrees with geological and field observations. However, if we define the fault zone thickness as the region where strain rate varies from a nearly constant value to a localized bell-shaped profile, the damage zone surrounding the fault core should be included. This means that would effectively increase the range of $T$ by at least a factor of 100.

The scaling between $D_o$ and fault zone thickness has interesting implications for interpretation of high velocity friction experiments. Indeed, the experimental setup of these tests is very different from velocity stepping experiments carried out with bare or relatively thin surfaces. Results from laboratory high velocity friction experiments show that fault zone thickness increases with slip velocity, but they are unable to constrain this relation because gouge escapes from the testing machine in most cases. Finally, in high velocity friction experiments, damage is created off-fault (see HIROSE AND BYSTRICKY, 2007) and therefore the definition itself of $T$ is not straightforward. We emphasize that the likely range of the critical slip weakening distance inferred from laboratory experiments remains poorly constrained. Bare surface, low velocity and high velocity friction experiments represent different proxies for a realistic fault zone. The paucity of detailed laboratory data on fault gouge and the incomplete understanding of laboratory observations from high and lower speed friction complicates attempts of bridging the gap between laboratory experiments and natural fault zones.

**Acknowledgements:** We thank two anonymous reviewers and E. Fukuyama for comments that helped to improve the manuscript.

## 8. References

AMPUERO, J.-P. and A. RUBIN (2008), Earthquake nucleation on rate and state faults –Aging and slip laws, *J. Geophys. Res., 113*, B01302, 10.1029/2007JB005082.

ANDO, R., and T. YAMASHITA (2007), Effects of mesoscopic-scale fault structure on dynamic earthquake ruptures: Dynamic formation of geometrical complexity of earthquake faults, *J. Geophys. Res., 112*, B09303, 10.1029/2006JB004612.

ANDREWS, D. J. (1976a), Rupture propagation with finite stress in antiplane strain, *J. Geophys. Res.*, **81**, 3575-3582.

ANDREWS, D. J. (1976b), Rupture velocity of plane strain shear cracks. J. Geophys. Res. 81, No. 32, 5679 – 5687.

ARBOLEYA, M. L., and T. ENGELDER (1995), Concentrated slip zones with subsidiary shears: their development on three scales in the Cerro Brass fault zone, Appalachian valley and ridge, *J. Struct. Geol.*, 17(4), 519-532.

BARENBLATT, G. I. (1959), The formation of brittle cracks during brittle fracture. General ideas and hypotheses. Axially-symmetric cracks. *Appl. Math. Mech. 23*, 1273–1282.

BEELER N. M., TULLIS T.E., and WEEKS J. D. (1994), The roles of time and displacement in the evolution effect in rock friction, *Geophys. Res. Lett., 21*,1987-90.

BEELER, N. M, TULLIS, T. E., BLANPIED, M. L., and WEEKS, J. D. (1996), Frictional behavior of large displacement experimental faults, *J. Geophys. Res., 101*, 8697-8715.

BEELER, N. M, TULLIS, T. E., and D. L. GOLDSBY, J. D. (2008), Constitutive relationships and physical basis of fault strength due to flash heating *J. Geophys. Res.*, 113, B01401, 10.1029/2007JB004988

Bhat, H. S. Olives, M., Dmowska, R. and J. R. Rice (2007) Role of fault branches in earthquake rupture dynamics, *J. Geophys. Res* 112, B11309, doi:10.1029/2007JB005027

BILLI, A. and F. STORTI (2004), Fractal distribution of particle size in carbonate cataclastic rocks from the core of a regional strike-slip fault zone, *Tectonophys., 384, 115-128.*

BIZZARRI A., M. COCCO, D. J. ANDREWS, and E. BOSCHI (2001), Solving the dynamic rupture problem with different numerical approaches and constitutive laws, *Geophys. J. Int.*, *144*, 656-678.

BIZZARRI, A., COCCO, M. (2003), Slip-weakening behavior during the propagation of dynamic ruptures obeying to rate- and state dependent friction laws. *J. Geophys. Res. 108*, 2373, 10.1029/2002JB002198.

BIZZARRI A., and M. COCCO (2006a), A thermal pressurization model for the spontaneous dynamic rupture propagation on a 3-D fault: Part I – Methodological approach, J. Geophys. Res., 111, B05303, 10.1029/2005JB003862

BIZZARRI A., and M. COCCO (2006b), A thermal pressurization model for the spontaneous dynamic rupture propagation on a 3-D fault: Part II – Traction evolution and dynamic parameters, J. Geophys. Res., 111, B05304, 10.1029/2005JB003864.

BOATWRIGHT, J., COCCO, M. (1996), Frictional constraints on crustal faulting. J. Geophys. Res. 101 (B6), 13895– 13909.

BOETTCHER, M. S., and C. MARONE (2004), The effect of normal force vibrations on the strength and stability of steadily creeping faults, *J. Geophys. Res.,* 109, B0340610.1029/2003JB002824.

BOITNOTT, G. N., BIEGEL, R. L., SCHOLZ, C. H., YOSIOKA, N. and WANG, W. (1992), Micromechanics of rock friction 2: quantitative modeling of initial friction with contact theory. *Geophys. Res., 97*, 8965-8978.

BOWDEN, F. P. and TABOR, D. (1950), *The Friction and Lubrication of Solids*. Part I. Oxford: Clarenden Press.

BURRIDGE, R. and KNOPOFF, L. (1967), Model and theoretical seismicity, *Bull. Seism. Soc. Am., 57*, 341–371 (1967).

CASHMAN, S.M., BALDWIN, J.N., CASMAN, K.V., SWANSON, K., and CRAWFORD, R. (2007), Microstructures developed by coseismic and aseismic faulting in near-surface sediments, San Andreas fault, *California: Geology*, *35*, 611–614, 10.1130/G23545A.1.

CHESTER, F.M., J.P. EVANS, and R.L. BIEGEL (1993), Internal structure and weakening mechanisms of the San Andreas fault, *J. Geophys. Res., 98*, 771-786.

COCCO, M., and BIZZARRI, A. (2002), On the slip-weakening behavior of rate- and state-dependent constitutive laws. *Geophys. Res. Lett.* 29 (11), 1– 4.

COCCO M. and E. TINTI (2008), Scale dependence in the dynamics of earthquake propagation: evidence from seismological and geological observations, *Earth Planet. Sci. Lett.*, in press.

COCCO M., E. TINTI, C. MARONE and A. PIATANESI (2008), Scaling of slip weakening distance with final slip during dynamic earthquake rupture, PAGEOPH, this issue.

COWAN, D. S. (1999), Do faults preserve a record of seismic slip? A field geologist's opinion, *J. Struct. Geol.*, 21, 995-1001.

DI TORO, G., NIELSEN, S., PENNACCHIONI, G. (2005). Earthquake rupture dynamics frozen in exhumed ancient faults. *Nature*, 436, 1009-1012.

DI TORO, G., HIROSE, T., NIELSEN, S., PENNACCHIONI, G., and T. SHIMAMOTO (2006). Natural and Experimental Evidence of Melt Lubrication of Faults During Earthquakes, *Science*, *311*. 647-649, 10.1126/science.1121012.

DIETERICH JH. (1972), Time-dependent friction in rocks. *J. Geophys. Res.* 77:3690-97.

DIETERICH JH. (1979), Modeling of rock friction: 1. Experimental results and constitutive equations. *J. Geophys. Res.* 84:2161-68.

DIETERICH, J.H. (1981), Constitutive properties of faults with simulated gouge, in *Mechanical Behavior of Crustal Rocks, Geophys. Mono. Ser. vol 24,* edited by N.L. Carter, M. Friedman, J.M. Logan, and D.W. Stearns, AGU Washington DC, 103-120.

DIETERICH JH. (1992), Earthquake nucleation on faults with rate and state-dependent friction. *Tectonophys*. 211:149-78.

DOWSON, D. (1979), History of Tribology, Longman, New York

FRYE, K. M., and C. MARONE (2002), The effect of humidity on granular friction at room temperature, *J. Geophys. Res., 107*, 10.1029/2001JB000654.

FUKUYAMA, E. and MIKUMO, T. (2007), Slip-weakening distance estimated at near-fault stations, *Geophys. Res. Lett., 34*, :10.1029/2006GL029203.

FUKUYAMA, E., MIKUMO, T., and OLSEN, K. B. (2003), Estimation of the Critical Slip-Weakening Distance: Theoretical Background, *Bull. Seism. Soc. Am.* 93, 1835-1840; 10.1785/0120020184.

GUATTERI, M., P. SPUDICH, and G. C. BEROZA (2001), Inferring rate and state friction parameters from a rupture model of the 1995 Hyogo-ken Nanbu (Kobe) Japan earthquake, *J. Geophys. Res., 106*, 26,511 – 26,521.

HIROSE T., and M. BYSTRICKY (2007), Extreme dynamic weakening of faults during dehydration by coseismic shear heating, *Geophys. Res. Lett., 34*, L14311, :10.1029/2007GL030049.

HIROSE, T., and SHIMAMOTO, T. (2005), Slip-weakening distance of faults during frictional melting as inferred from experimental and natural pseudotachylytes, *Bull. Seism. Soc. Am., 95*, 1666-1673, 10.1785/0120040131.

IDA, Y. (1972), Cohesive force across the tip of a longitudinal–shear crack and Griffith's specific surface energy. *J. Geophys. Res., 77*, 3796-3805.

IDE, S., and M. TAKEO (1997), Determination of constitutive relations of fault slip based on seismic wave analysis, *J. Geophys. Res, 102*, 27,379-27,391.

IKARI, M., SAFFER, D. M., and C. MARONE (2007), Effect of Hydration State on the Frictional Properties of Montmorillonite-based Fault Gouge, *J. Geophys. Res,* 112, B06423 10.1029/2006JB004748.

KARNER, S. L. and C. MARONE (2001), Frictional restrengthening in simulated fault gouge: effect of shear load perturbations, *J. Geophys. Res,, 106,* 19319-19337.

KNUTH, M., and C. MARONE (2007), Friction of sheared granular layers: the role of particle dimensionality, surface roughness, and material properties, *Geochem. Geophys. Geosyst.*, 8, Q03012, :10.1029/2006GC001327.

LAPUSTA N. and J.R. RICE (2003), Nucleation and early seismic propagation of small and large events in a crustal earthquake model, *J. Geophys. Res., 108*, 2205, 10.1029/2001JB000793.

LIU, Y and RICE, J.R. (2007), Spontaneous and triggered aseismic deformation transients in a subduction fault model, *J. Geophys. Res.*, *112*, 10.1029/2007JB004930.

LOGAN, J. M., M. FRIEDMAN, N. HIGGS, C. DENGO, and T. SHIMAMODO (1979), Experimental studies of simulated fault gouges and their application to studies of natural fault zones, *in Analysis of Actual Fault Zones in Bedrock, US Geol. Surv. Open File Rep., 1239*, 305-343.

MAIR, K., FRYE, K. M., and C. MARONE (2002), Influence of grain characteristics on the friction of granular shear zones, *J. Geophys. Res., 107* (10), 2219, 10.1029/2001JB000516.

MAIR, K., and HAZZARD, J.F. (2007), Nature of stress accommodation in sheared granular material: Insights from 3D numerical modelling, *Earth and Planetary Science Letters*, *259*, 469-485, 10.1016/j.epsl.2007.05.006

MAIR, K., and C. MARONE (1999), Friction of simulated fault gouge for a wide range of velocities and normal stress, *J. Geophys. Res., 104*(B12), 28,899-28,914.

MANDL, G., L. N. J. DE Jong, and A. MALTHA (1977), Shear zones in granular material, an experimental study of their structure and mechanical genesis, *Rock Mech.*, 9, 95-144.

MARONE, C. (1998), Laboratory-derived friction constitutive laws and their application to seismic faulting, *Ann. Rev. Earth Planet. Sci., 26*, 643-696.

MARONE, C. and B. KILGORE (1993), Scaling of the critical slip distance for seismic faulting with shear strain in fault zones, *Nature*, *362*, 618-622.

MARONE, C., C. B. RALEIGH, and C. H. SCHOLZ (1990), Frictional behavior and constitutive modeling of simulated fault gouge, *J. Geophys. Res., 95*(B5), 7007-7025.

MARONE, C., C. H. SCHOLZ, and R. BILHAM (1991), On the mechanics of earthquake afterslip, *J. Geophys. Res., 96*, 8441-8452.

MIKUMO, T., K. B. OLSEN, E. FUKUYAMA, and Y. YAGI (2003), Stress-breakdown time and slip-weakening distance inferred from slip-velocity functions on earthquake faults, *Bull. Seismol. Soc. Am.*, *93*, 264-282.

S. NIELSEN, G. DI TORO, T. HIROSE, and T. SHIMAMOTO (2008), Frictional melt and seismic slip, *J. Geophys. Res.,* 113, B01308, 10.1029/2007JB005122.

NIEMEIJER, A.R. and SPIERS, C.J. (2006), Velocity dependence of strength and healing behaviour in simulated phyllosilicate-bearing fault gouge. *Tectonophysics, 427, 231-253,* 10.1016/j.tecto.2006.03.048.

OHNAKA, M. (1973), Experimental studies of stick-slip and their application to the earthquake source mechanism, *J. Phys. Earth*, *21*, 285-303.

OHNAKA, M. (2003), A constitutive scaling law and a unified comprehension for frictional slip failure, shear fracture of intact rock, and earthquake rupture, *J. Geophys. Res.*, 108(B2), 2080, 10.1029/2000JB000123.

OHNAKA M, KUWAHARA Y. (1990), Characteristic features of local breakdown near a crack-tip in the transition zone from nucleation to dynamic rupture during stick-slip shear failure. *Tectonophys.*, *175*,197-220.

PALMER, A. C., and RICE, J. R. (1973), The growth of slip surfaces in the progressive failure of over- consolidated clay. *Proc. R. Soc. London* Ser. A **332**, 527-548.

PERFETTINI, H. and J.-P. AVOUAC (2004), Stress transfer and strain rate variations during the seismic cycle, *J. Geophys. Res., 109*, 10.1029/2003JB002917.

RABINOWICZ E. (1951), The nature of static and kinetic coefficients of friction. *J. Appl. Phys. 22*, 1373-1379.

RABINOWICZ E. (1958), The intrinsic variables affecting the stick-slip process. *Proc. Phys. Soc. (London)* 71:668-675.

RICE, J. R. (1993), Spatio-temporal complexity of slip on a fault, J. Geophys. Res., 98, 9885 – 9907.

RICE, J. R. (2006), Heating and weakening of faults during earthquake slip, *J. Geophys. Res.,* 111(B05311).

RICE J.R., and A. L. RUINA (1983), Stability of steady frictional slipping. *J. Appl. Mech.* 105, 343-349.

RICHARDSON, E. and C. MARONE (1999), Effects of normal stress vibrations on frictional healing, *J. Geophys. Res., 104,* 28,859-28,878.

RUINA, A.L. (1983), Slip instability and state variable friction laws., *J. Geophys. Res.* 88 (B12), 10359–10370.

RUTTER E. H., MADDOCK R. H., HALL S. H., and WHITE S. H. (1986), Comparative microstructure of natural and experimentally produced clay bearing fault gouges, *Pageoph*, *24*, 3-30.

SAVAGE, H., and C. MARONE (2007), The Effects of Shear Loading Rate Vibrations on Stick-Slip Behavior in Laboratory Experiments, *J. Geophys. Res,* 112, B02301, 10.1029/2005JB004238.

SEGALL, P. and RICE, J. R. Dilatancy (1995), compaction, and slip instability of a fluid infiltrated fault. *J. Geophys. Res.*, *100*, 22,155-22,173.

SCHOLZ C. H. (1998) Earthquakes and friction laws, *Nature, 391,* 37-42.

SCHOLZ C. H. (2002), *The Mechanics of Earthquakes and Faulting, 3rd ed.*, Cambridge, pp. 471.

SCHOLZ C. H., MOLNAR P., and JOHNSON T. (1972), Detailed studies of frictional sliding of granite and implications for the earthquake mechanism. *J. Geophys. Res.* 77:6392-406.

SIBSON, R. H. (2003), Thickness of the seismic slip zone, *Bull. Seism. Soc. Am. 93*(3), 1169-1178.

SLEEP N.H. (1997), Application of a unified rate and state friction theory to the mechanics of fault zones with strain localization. *J. Geophys. Res.*, *102*, 2875-95.

SOLUM J. G., van der PLUIJM B. A., PEACOR D. R., and WARR L. N. (2003), Influence of phyllosilicate mineral assemblages, fabrics, and fluids on the behavior of the Punchbowl fault, southern California, *J. Geophys. Res.*, *108*, 10.1029/2002JB001858,.

SPUDICH, P., and GUATTERI, M. (2004), The effect of bandwidth limitations on the inference of earthquake slip-weakening distance from seismograms, *Bull. Seism. Soc. Am.*, *94,* 2028-2036, 10.1785/0120030104

STORTI, F., BILLI, A., and F. SALVINI. (2003), Particle size distributions in natural carbonate fault rocks: insights for non-self-similar cataclasis, *EPSL, 206, 173-186*.

TINTI, E., A. BIZZARRI, A. PIATANESI, and M. COCCO (2004), Estimates of slip weakening distance for different dynamic rupture models, *Geophys. Res. Lett.*, 31, L02611, 10.1029/2003GL018811.

TINTI, E., P. SPUDICH, and M. COCCO (2005), Earthquake fracture energy inferred from kinematic rupture models on extended faults, *J. Geophys. Res.*,110, B12303, 10.1029/2005JB003644.

TULLIS, T. E. (1988), Rock friction constitutive behavior from laboratory experiments and its implications for an earthquake prediction field monitoring program, *Pure Appl. Geophys.*, *126*, 555-588.

TULLIS, T. E. (1996), Rock friction and its implications for earthquake prediction examined via models of Parkfield earthquakes, in *Earthquake Prediction: the Scientific Challenge*, ed. by Leon Knopoff, *Proc. Natl. Acad. Sci. USA, 93*, 3803-3810.

TULLIS T. E, and WEEKS J. D. (1986), Constitutive behavior and stability of frictional sliding of granite. *Pure Appl. Geophys.* 124:383-414.

van der PLUIJM, B. A., HALL, C. M., VROLIJK, P. J., PEVEAR, D. R., and COVEY, M.C. (2001), The dating of shallow faults in the Earth's crust, *Nature*, *412*, 172-175, 10.1038/35084053.

ZIV, A. (2007), On the nucleation of creep and the interaction between creep and seismic slip on rate- and state-dependent faults, *Geophys. Res. Lett*, 34, 10.1029/2007GL030337.

**Figure captions**

**Figure 1.** (**a**) Slip weakening friction law in which friction decreases from a static value $\mu_s$ to a kinetic value $\mu_k$ linearly over slip distance $s_k$. Kinetic friction is independent of slip velocity. (**b**) Idealized representation of the increase in static friction with the time of contact $\mathbf{t_c}$, so-called *frictional healing*, showing approximately linear healing with the logarithm of contact age. (**c**) Rate and state friction law in which static and kinetic friction, and frictional healing, are special cases of a more general behavior. Friction varies with slip velocity, time of stationary contact, and recent memory of sliding conditions including velocity, normal stress, chemical environment, and temperature. The parameters $L$ and $d_o$ are the critical friction distance and the dynamic slip weakening distance, respectively, for a single frictional surface. (**d**) Idealized shear traction evolution curve for a dynamic rupture on a fault zone of finite width. The parameters $\tau_o$ (initial stress), $\tau_y$ (yield stress), and $\tau_f$ (dynamic frictional strength) define stress drop and strength excess. The shaded region represents the seismological fracture energy, which is referred to as breakdown work $W_b$. The parameters $D_a$, $D_{cb}$, $D_o$ and $D_{tot}$ are the slip at peak strength, the fault zone critical friction distance, the effective dynamic slip weakening distance, and the total slip, respectively, for a fault zone of finite thickness.

**Figure 2.** Idealized representations of friction contact junctions for clean surfaces (a & b) and surfaces separated by wear (gouge) materials (c-e). (a & b): Section and plan views of an asperity contact junction of diameter 2r formed during (a) static loading and (b) after sliding a distance s. Shaded areas represent the true area of contact, which decreases with slip and is reformed after a critical time. (c) Cross-section of a gouge zone between rough surfaces showing 3-D contact geometry of idealized wear particles. (d) Section view of idealized, boundary-parallel contact junctions within the model fault zone. Each contact has diameter 2r. (e) Contact geometry after the upper boundary is displaced by a slip distance x; each contact slips a distance s. For clean surfaces the transition from static to kinetic friction is determined by contact junction properties, whereas for a wear zone the transition is determined by the number of contacts, contact junction properties, and particle interactions.

**Figure 3.** Fault zone model. Idealized crustal fault zone of thickness T. Fracture density increases toward fault zone, which includes multiple sub-parallel slip surfaces. Fault zone boundary is driven by remote loading $v_{lp}$ and 1D stiffness $K_{ext}$. (inset) Enlargement of fault zone showing slip surfaces separated by distance h; half-thickness of fault zone is T/2. Left side is shear zone boundary, dotted line is shear zone center. Each slip surface obeys the friction constitutive law. Fault zone shear is driven by boundary shear and elastofrictional interaction between surfaces. Thin lines denote elastic connection between surfaces (equivalent to leaf-springs) characterized by $K_{int}$.

**Figure 4**. Slip vs. frictional traction for a single surface (thin line labeled Ref. in each panel) and for the center of a 24 cm-thick shear zone composed of 40 surfaces. In each case the loading velocity $v_{lp}$ (Figure 3) is subject to a step increase from 1 micron/s to 1cm/s. Friction parameters are same for all surfaces (see Table 1) and frictional state evolves following the Dieterich law (a) or the Ruina law (b). Panel a shows friction parameters $L$ and $d_o$ for a single surface are the corresponding parameters for a shear zone of finite width. $D_{cb}$ is the effective critical friction distance and $D_o$ is the effective dynamic slip weakening distance, respectively, defined by net slip across a shear zone.

**Figure 5**. Time vs. friction (thick line) and velocity (thin line) following an increase in loading velocity from 1 micron/s to 1 cm/s for a shear zone 12 cm thick composed of 20 surfaces. $D_c$' is the slip at peak velocity.

**Figure 6.** Slip (a) and time (b) vs. frictional traction following an increase in loading velocity from 1 micron/s to 1 cm/s for a single surface (curve labeled Ref.) and for a shear zone 60 cm thick containing 100 surfaces. Friction evolution is shown for various positions within the shear zone. Labels denote surface number: 10 is near the shear zone boundary and 50 is at the center, see Figure 3). Friction parameters are same for all surfaces (see Table 1) and frictional state evolves following the Ruina law.

**Figure 7**. Slip vs. frictional traction following velocity steps of different sizes for a 72 cm thick shear zone containing 120 surfaces. $D_a$, the slip at peak friction, is shown for one case in each panel. $D_a$ is roughly independent of acceleration history for the Dieterich law (a), but decreases with increasing velocity step size for the Ruina evolution law (b). Labels denote ratio of final to initial slip velocity.

**Figure 8**. Slip at peak friction $D_a$ vs. velocity jump size $\ln(v/v_o)$ for a variety of shear zone thicknesses. Labels in panel a denote number of surfaces in half width; Ref indicates a single frictional surface. The same symbols are used to indicate share zone width in both panels. For the Dieterich law, $D_a$ is nearly independent of velocity step size (a). For the Ruina law, $D_a$ decreases with increasing velocity step size for thick (>30 surfaces) shear zones (b).

**Figure 9**. Effective dynamic slip weakening $D_o$ vs. velocity jump size $\ln(v/v_o)$ for a variety of shear zone thicknesses. Labels in 9a denote number of surfaces in half width; Ref indicates a single frictional surface. The same symbols are used to indicate share zone width in both panels. (a) For the Dieterich law, $D_0$ increases with shear zone thickness and velocity step size. (b) Note that the difference $D_o$-$D_a$ increases with velocity jump size. (c) For the Ruina law, $D_0$ is nearly independent of velocity step size for thin (< 30 surfaces) shear zones but exhibits complex behavior for thick shear zones. (d) The difference $D_o$-$D_a$ is relatively insensitive to velocity jump size and show complex behavior.

**Figure 10**. Effective dynamic slip weakening $D_o$ and slip at peak friction $D_a$ vs. fault zone thickness for three different velocity jump sizes. For the Dieterich law, $D_a$ is nearly independent of jump size and increases with fault zone thickness (a), while $D_0$ increases with both fault zone thickness and increasing velocity jump size (c). For the Ruina law, $D_a$ decreases with increasing jump size and increases with increasing fault zone thickness (b), while $D_0$ exhibits complicated behavior with respect to both velocity jump size and fault zone thickness (d).

**Figure 11**. Effective dynamic slip weakening $D_o$ and slip at peak friction $D_a$ vs. intrinsic critical friction distance L for two fault zone thickness and two different velocity jump sizes. For the Dieterich law, both $D_a$ and $D_0$ are independent of velocity jump size, whereas $D_a$ and $D_0$ scale with fault zone width. For the Ruina law, both $D_a$ and $D_0$ scale weakly with velocity jump size and more strongly with fault zone width.

**Figure 12**. Slip profile and strain rate profile across the model fault zone for the Dieterich law (upper plots) and Ruina law (lower plots). Horizontal dashed lines represent center of the fault zone. Vertical dashed line and markers at shear zone boundary provide slip reference. Note non-linear slip distribution as a function of position, within the shear zone. Slip and strain rate are shown for the point at which the boundaries slid by an amount equal to $D_a$.

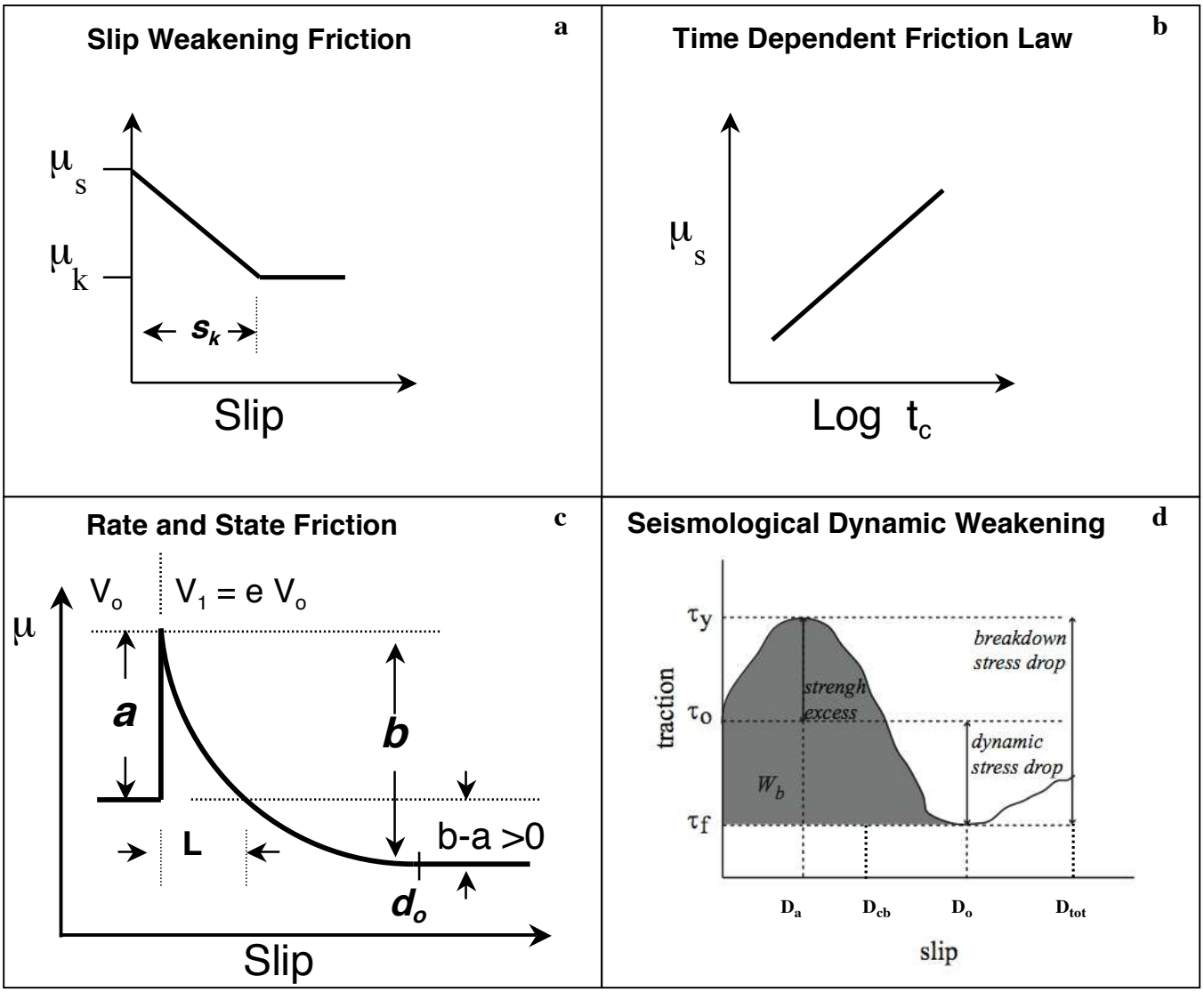


*Marone et al., Critical Slip Distance, 2008,* Figure 1.

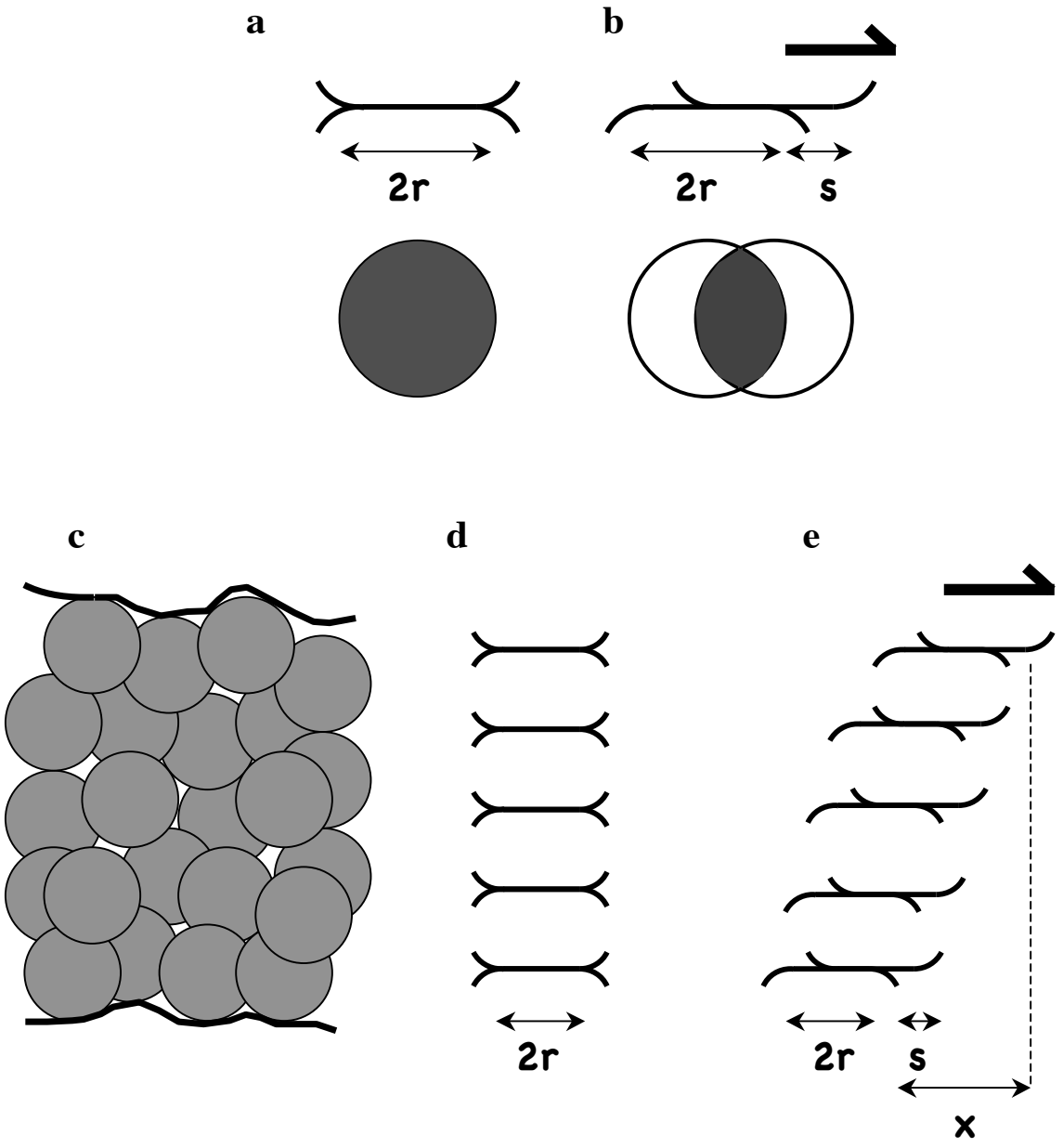


*Marone et al., Critical Slip Distance, 2008,* Figure 2.

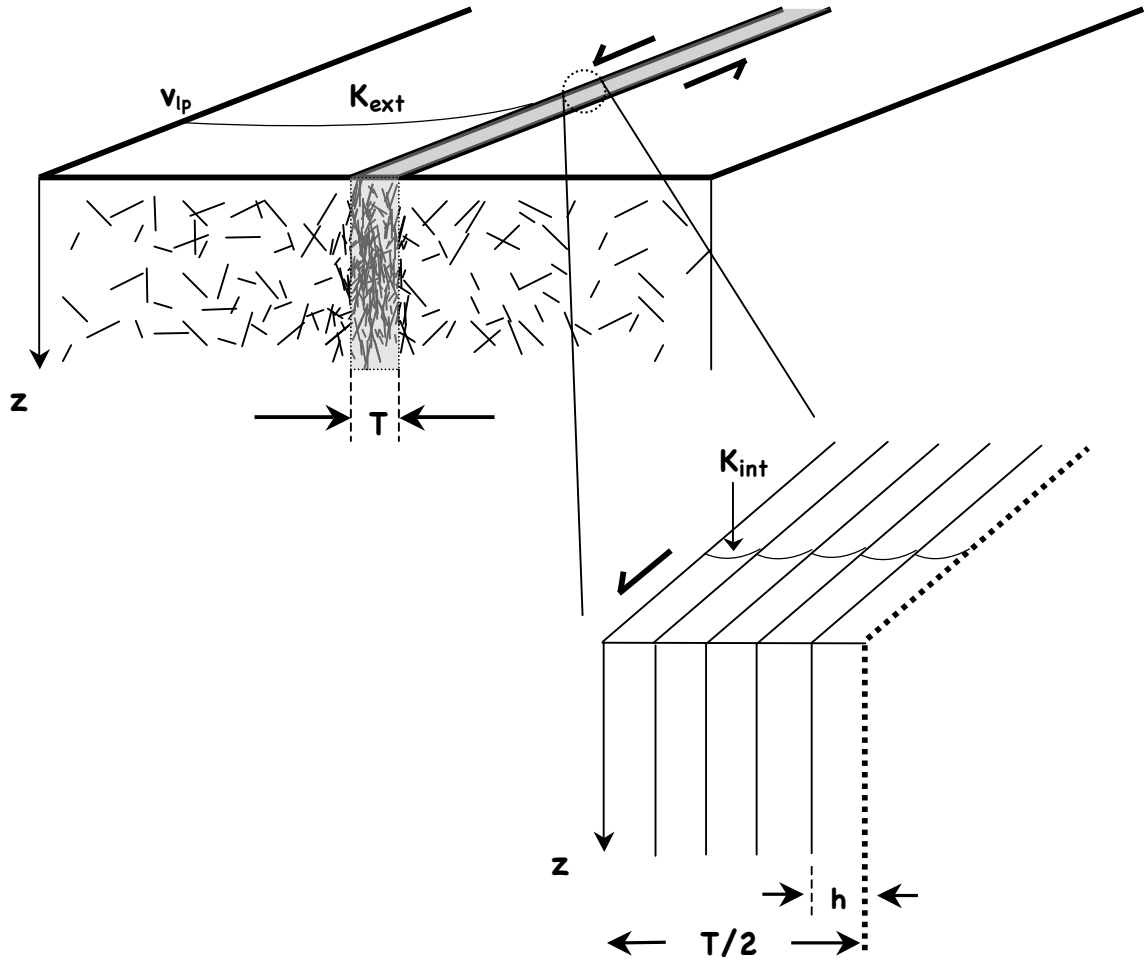


*Marone et al., Critical Slip Distance, 2008,* Figure 3.

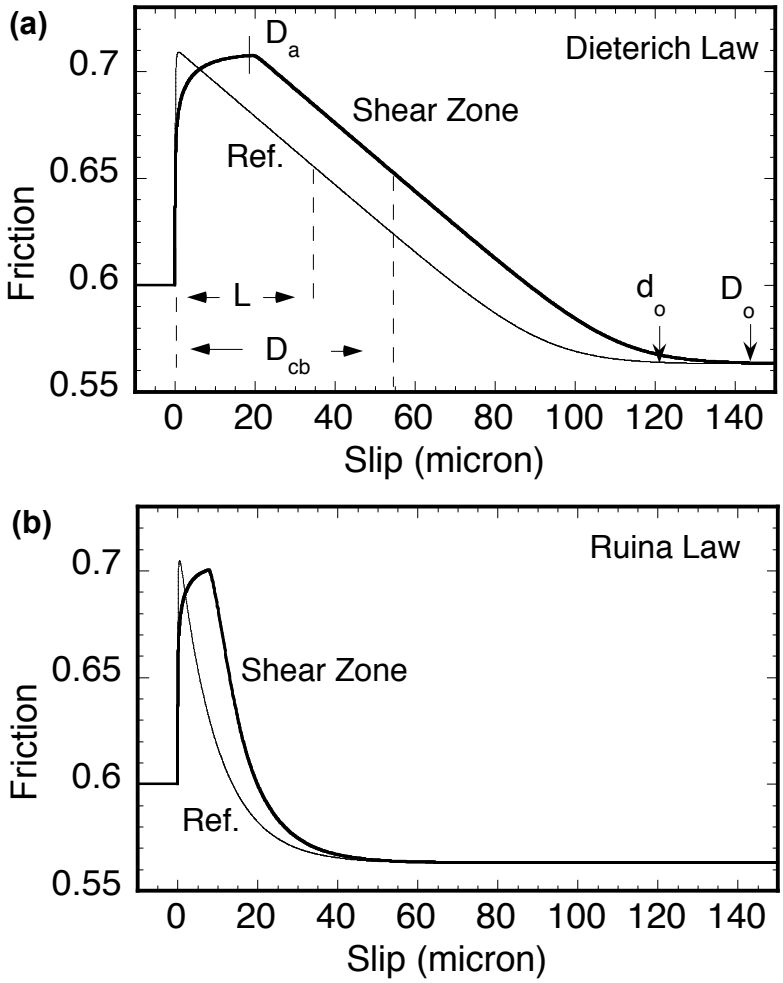


*Marone et al., Critical Slip Distance, 2008,* Figure 4.

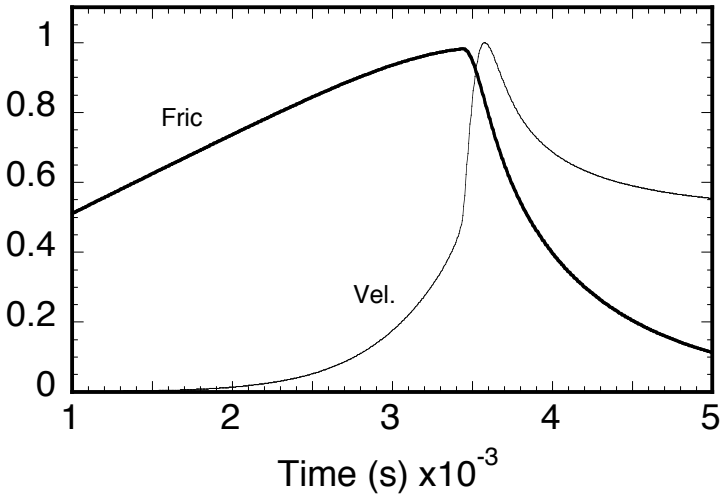


*Marone et al., Critical Slip Distance, 2008,* Figure 5.

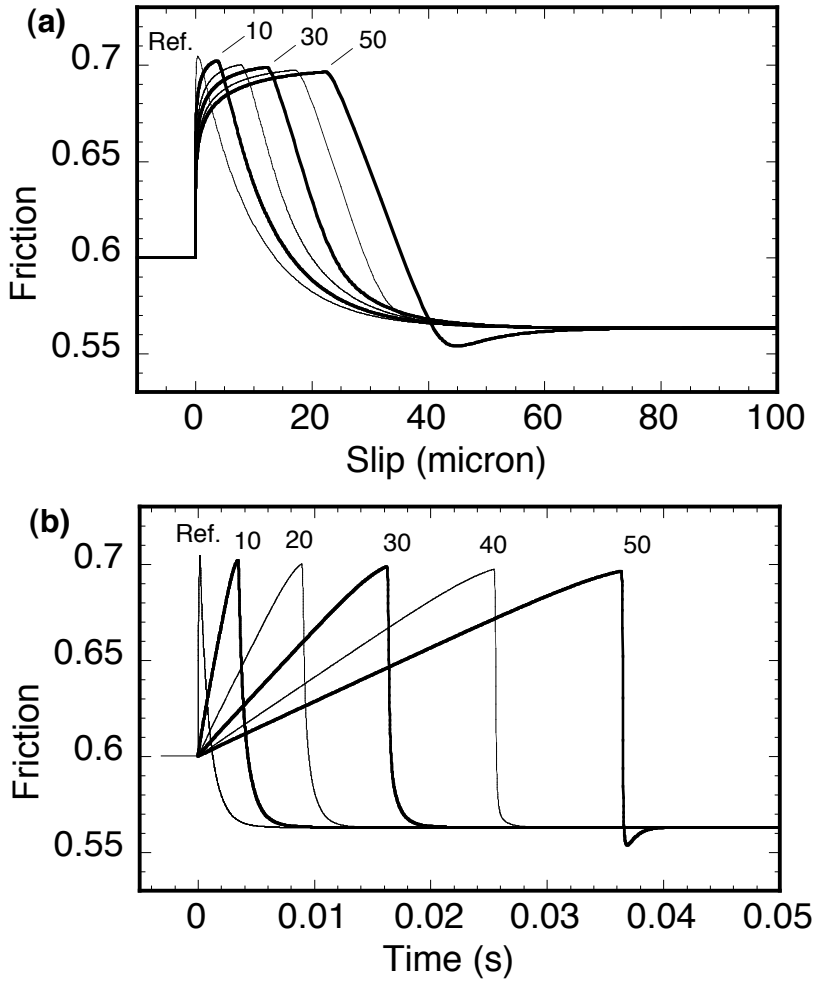


*Marone et al., Critical Slip Distance, 2008,* Figure 6.

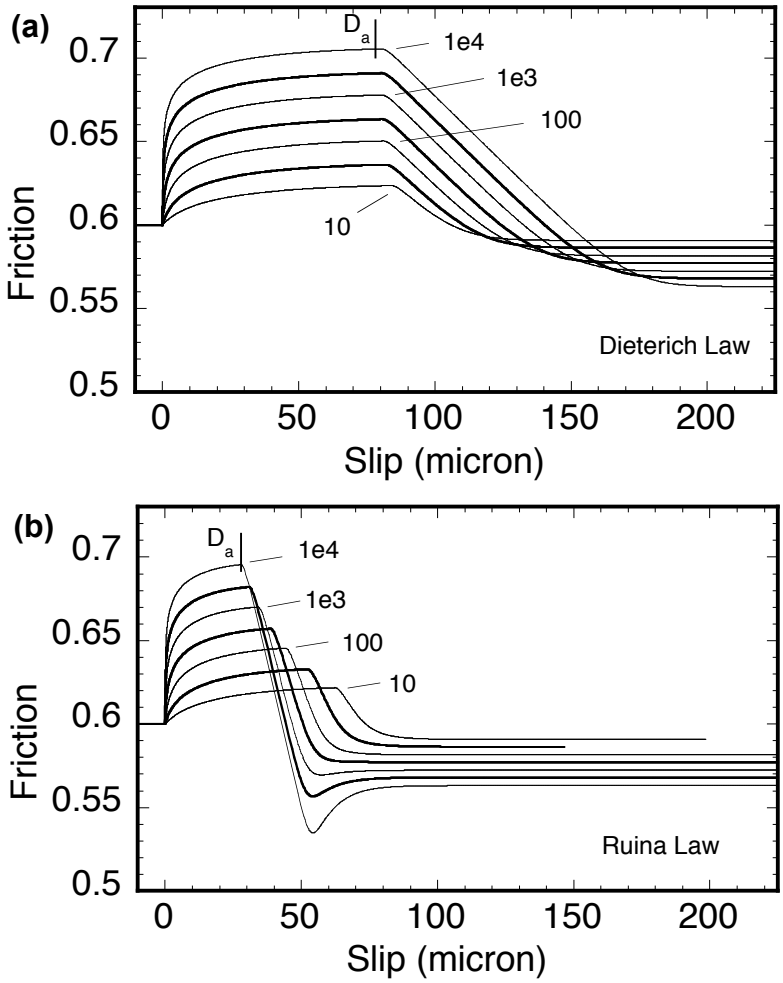


*Marone et al., Critical Slip Distance, 2008,* Figure 7.

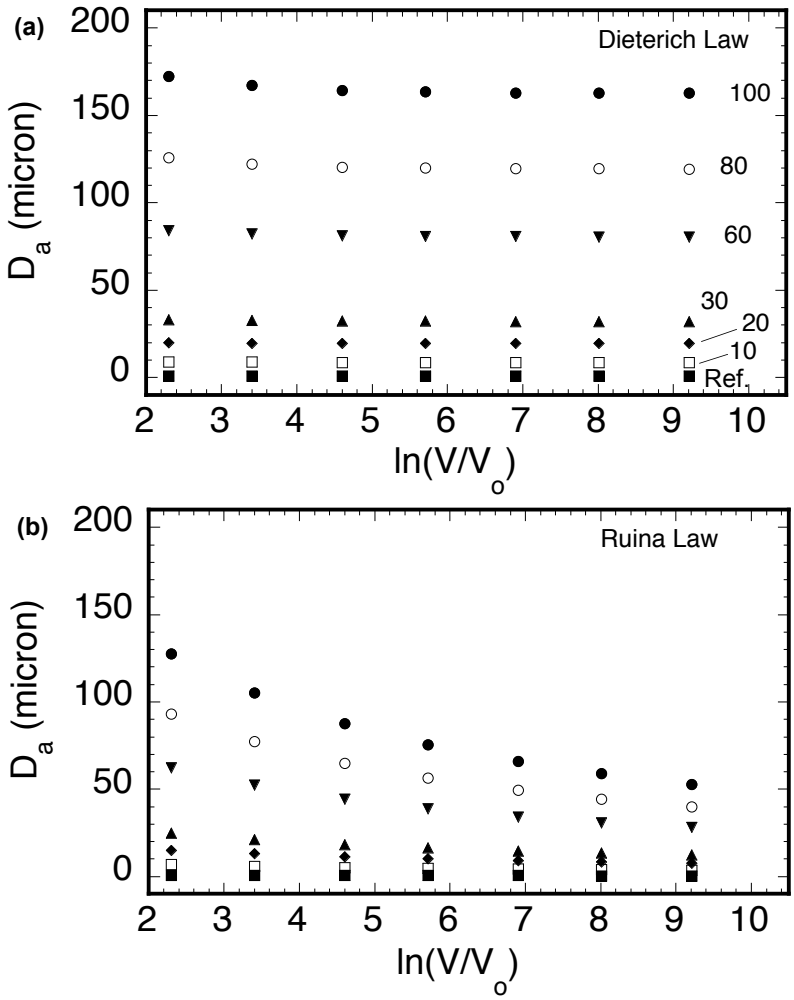


*Marone et al., Critical Slip Distance, 2008,* Figure 8.

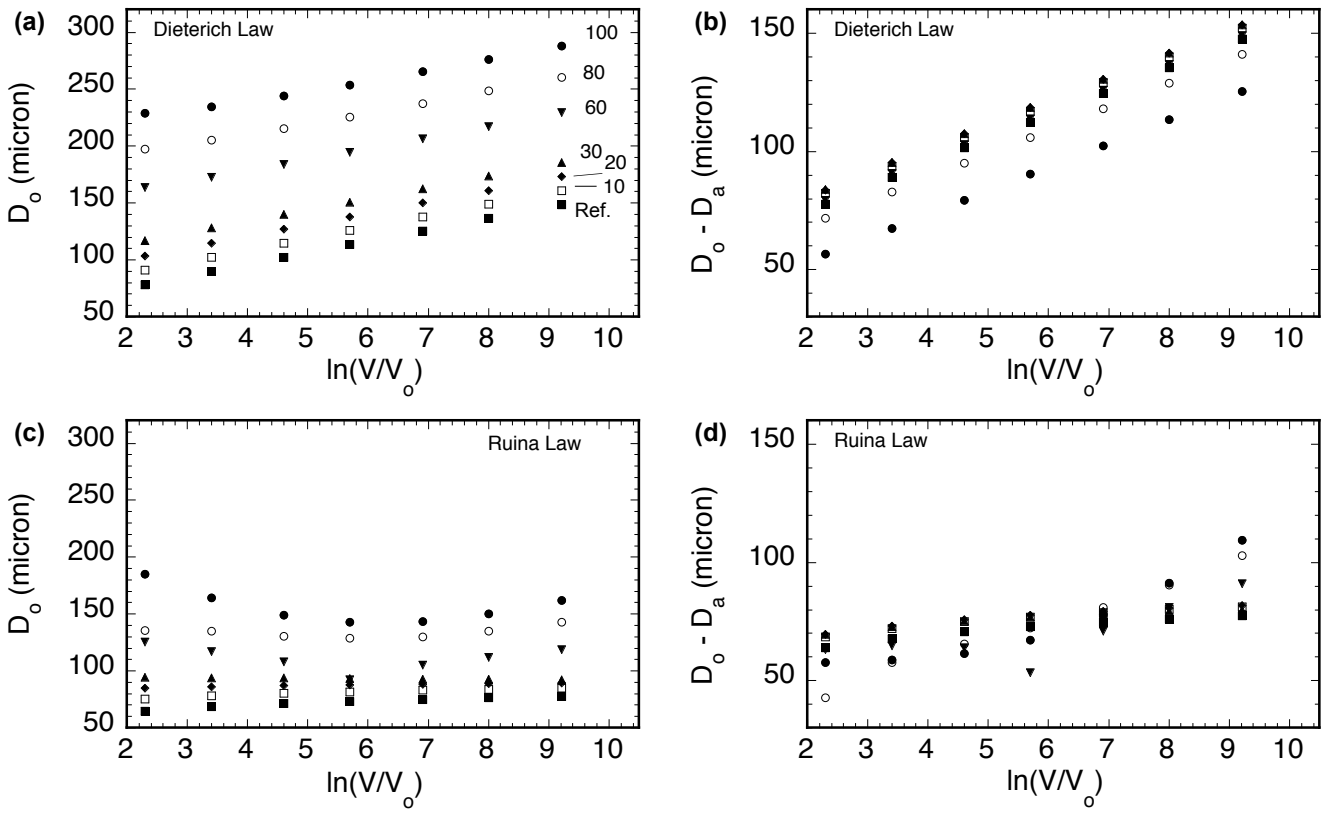


*Marone et al., Critical Slip Distance, 2008,* Figure 9.

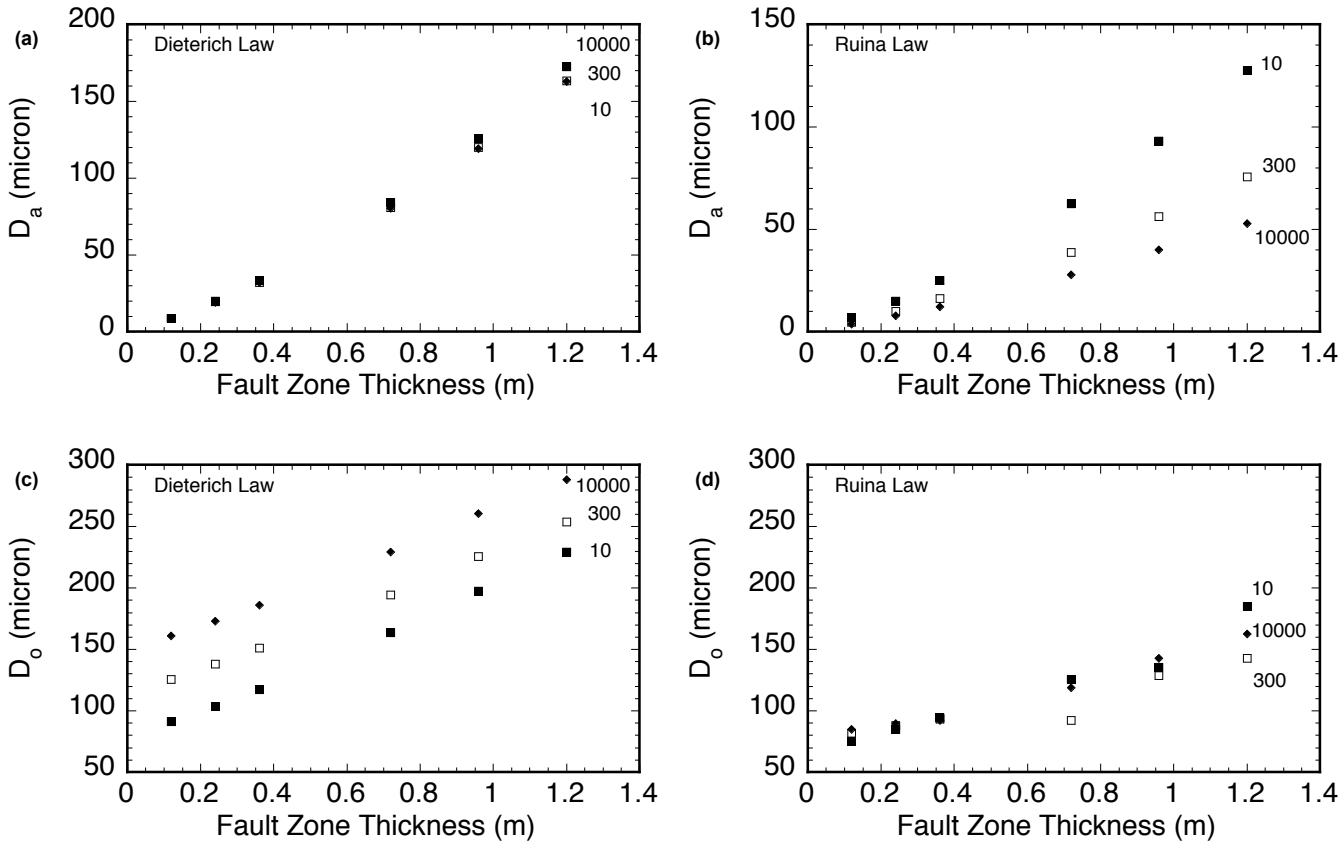


*Marone et al., Critical Slip Distance, 2008,* Figure 10.

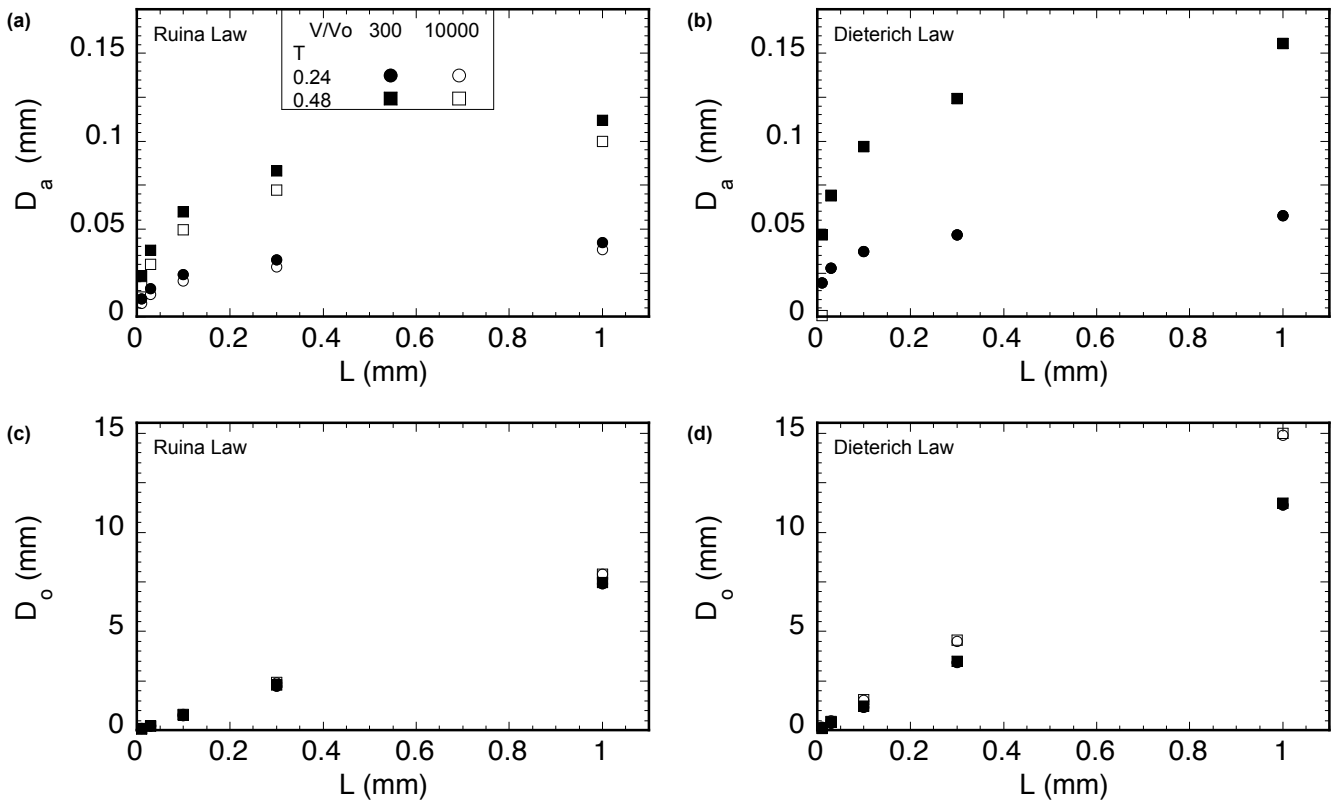


*Marone et al., Critical Slip Distance, 2008,* Figure 11.

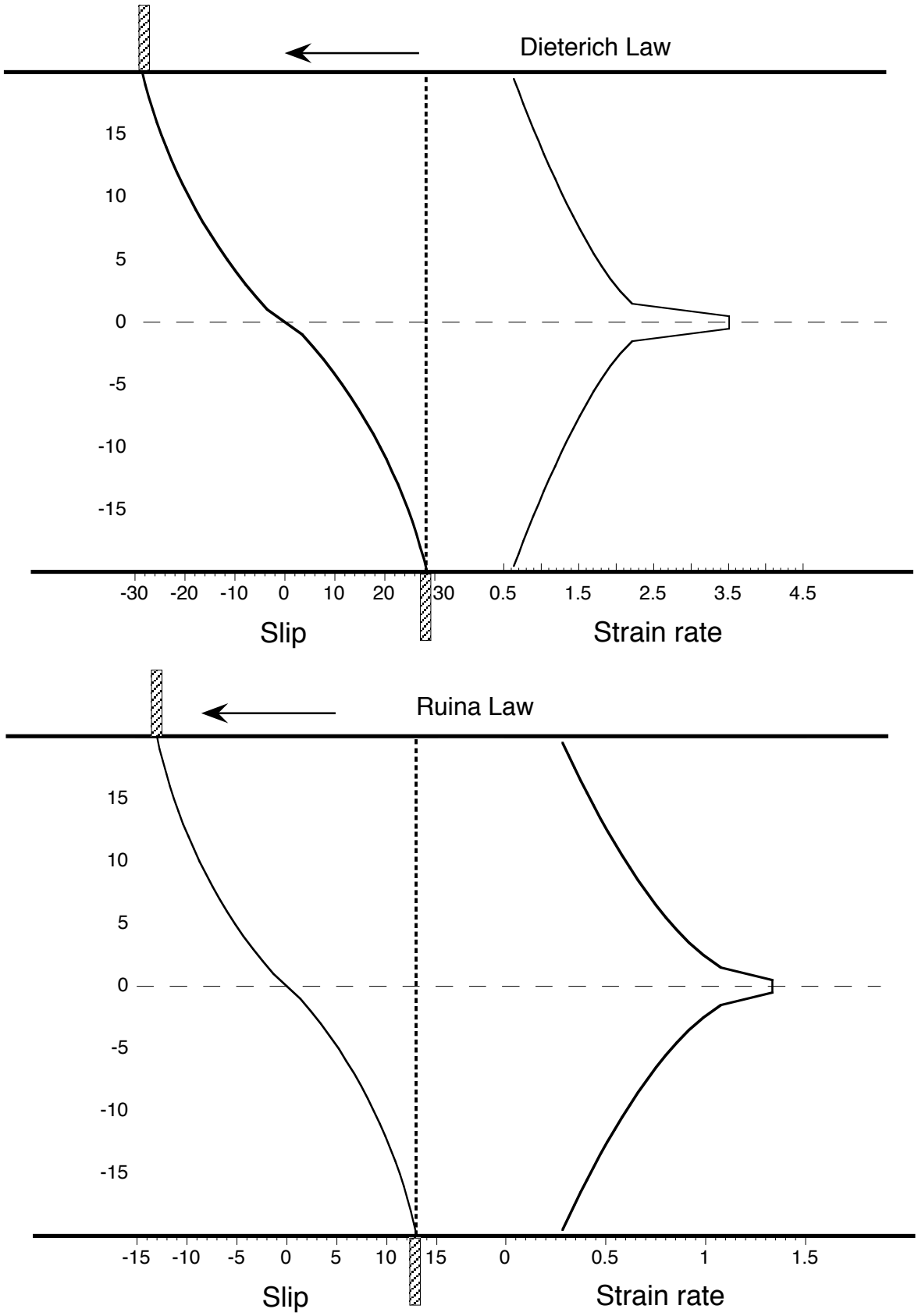


*Marone et al., Critical Slip Distance, 2008,* Figure 12.